Fluorescence characteristics of IC7-1, IC7-2, IC7-1 lactosome and IC7-2 lactosome

IC7-1, a lipophilic fluorophore with a cyclohexene ring in the interior of the polymethine chain of the ICG structure, had a maximum emission wavelength at 858 nm in chloroform (Table 1). IC7-2 with an unsymmetrical cyanine structure had a maximum emission wavelength at 897 nm in chloroform, which as expected was a longer emission wavelength compared with conventional NIR-dyes. In addition to maximum emission wavelength, other fluorescent properties of IC7-1 and IC7-2 in chloroform such as fluorescence spectrum, quantum yield, and extinction coefficient were also quite similar to those of IC7-1 lactosome and IC7-2 lactosome measured in water (Fig. 3, Table 1). In particular, IC7-1 and IC7-1 lactosome had sharp absorbance and emission spectra and a narrow Stokes shift, while IC7-2 and IC7-2 lactosome had broad absorption spectra and a relatively long Stokes shift.

The fluorescence characteristics of IC7-1, IC7-1 lactosome, IC7-2, and IC7-2 lactosome were compared with ICG as summarized in Table 1. Both IC7-1 and IC7-2 displayed longer absorbance, excitation, and emission wavelengths than ICG. IC7-1 and IC7-2 had higher quantum yields and molar extinction coefficients in chloroform than in methanol. IC7-1 lactosome had approximately 52 nm and 43 nm longer maximum absorbance and emission wavelengths and approximately 2.5 fold higher quantum yield and molar extinction coefficients compared with ICG. IC7-2 lactosome had a maximum emission wavelength that was 55 nm longer than IC7-1 lactosome and 98 nm longer than ICG.

Regarding photostability of the three probes, the absorbances of IC7-1 lactosome and IC7-2 lactosome were stable for 1 h under tungsten lamp irradiation (Fig. 4). On the other hand, the absorbance of ICG significantly decreased in a time-dependent manner ($p<0.0001$), and the normalized absorbance of ICG after 60 min was 61% of the 0 min value.

In vivo imaging study

Fluorescence images of tumor-bearing mice administered IC7-1 lactosome or IC7-2 lactosome are shown in Fig. 5a and b, respectively. The tumors of mice administered IC7-1 lactosome and IC7-2 lactosome were visible with both agents 6 h after administration. The fluorescence intensity at the tumor region of mice administered IC7-1 lactosome (Fig. 5c) and IC7-2 lactosome (Fig. 5d) gradually increased in a time-dependent manner reaching a peak 24 h after administration that was significantly greater than the fluorescence observed in the muscle and liver regions ($p< 0.05$). The fluorescence intensities of tumors 24 h after probe administration were 3.1 fold (IC7-1 lactosome) and 2.5 fold (IC7-2 lactosome) greater than those at the 0 h time point (immediately after probe administration). The intensities in the muscle region (the opposite side from the tumor) were relatively constant during the study, and the tumor-to-muscle fluorescence ratios 24 h after administration were 2.2±0.7 (IC7-1 lactosome) and 2.2±0.2 (IC7-2 lactosome). The tumor-to-liver fluorescence ratios 24 h after administration were 2.5±0.6 (IC7-1 lactosome) and 1.7±0.2 (IC7-2 lactosome), while the intensities in the liver region of the IC7-2 lactosome group were transiently high during the early imaging phase.

Discussion

In this study, two lipophilic NIR fluorescent agents, IC7-1 and IC7-2, were prepared and evaluated (Fig. 1). To enhance the utility of these agents for *in vivo* NIR optical tumor imaging, they were encapsulated in a lactosome formulation to take advantage of the ability of lactosomes to effectively target and deliver lipophilic compounds to tumor tissues. As expected, these fluorescent probes and their lactosome complexes displayed absorption, excitation, and emission spectra with red shifts (Fig. 3) as well as high photostability compared with ICG (Fig. 4). The IC7-1

Table 1 Optical properties of IC7-1, IC7-1 lactosome, IC7-2, IC7-2 lactosome, and ICG

Entry	Solvent	Abs_{max}	Ex_{max}	Em_{max}	Quantum yield	Extinction coefficient (M^{-1} cm^{-1})
IC7-1	$CHCl_3$	829	830	858	0.054	2.1×10^5
	MeOH	819	823	840	0.021	1.2×10^5
IC7-1 lactosome	H_2O	831	831	850	0.059	2.2×10^5
IC7-2	$CHCl_3$	781	805	897	0.008	9.2×10^4
	MeOH	790	883	932	0.001	2.6×10^4
IC7-2 lactosome	H_2O	830	844	905	0.014	6.0×10^4
ICG	H_2O	779	762	807	0.023	7.8×10^4

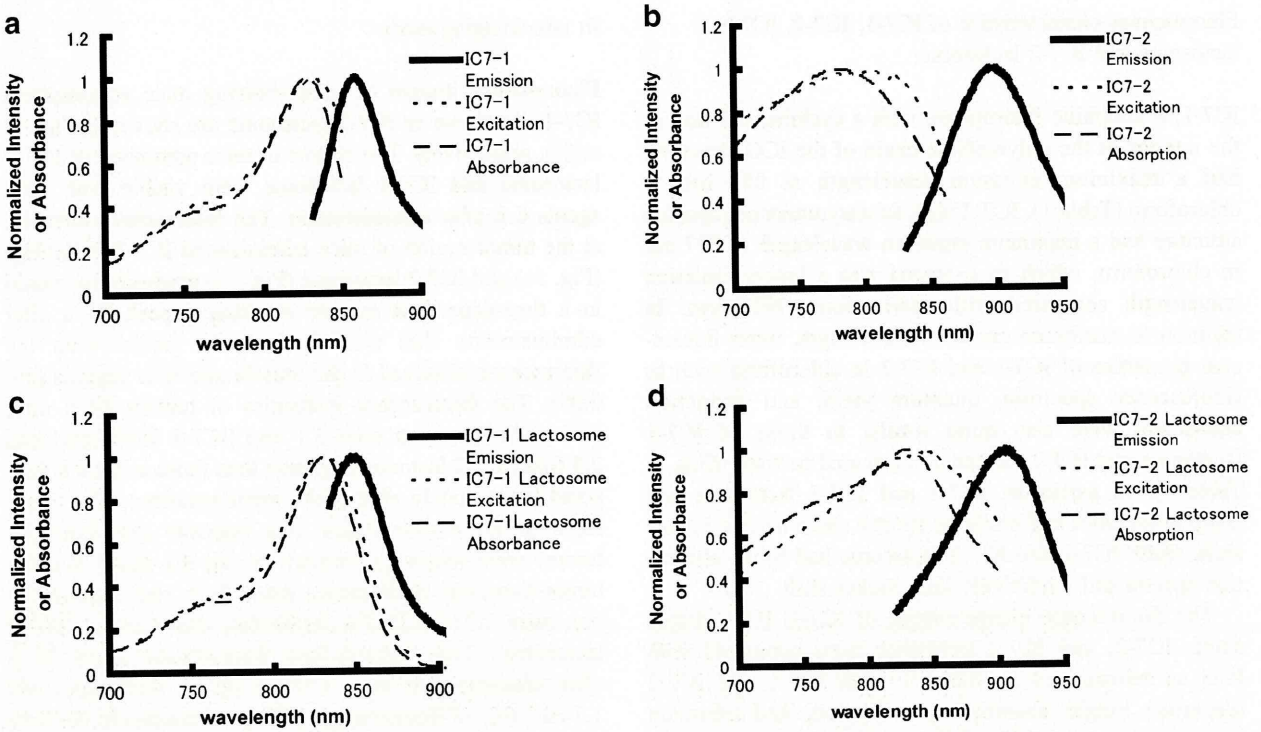

Fig. 3 Emission (*solid line*), excitation (*dotted line*) and absorption (*dotted solid line*) spectra of IC7-1 (**a**), IC7-2 (**b**), IC7-1 lactosome (**c**), and IC7-2 lactosome (**d**). The spectra for IC7-1 and IC7-2 were measured in chloroform and the spectra for IC7-1 lactosome and IC7-2 lactosome were measured in water

lactosome possessed a 2.5 fold higher quantum yield than ICG in aqueous solution (Table 1). In addition, IC7-1 lactosome and IC7-2 lactosome clearly allowed visualization of tumor tissue 6 h post-administration and showed significant fluorescence intensity in tumor tissue 24 h and 48 h after administration (Fig. 5).

In the design of IC7-1, a cyclohexene ring was incorporated into the interior of the polymethine chain of the ICG structure, because the added structural rigidity provided by a ring would lead to a red-shift of the emission and would increase the photostability and quantum yield in a lipophilic environment [13]. As a result of this modification, the emission spectra were elongated approximately 50 nm compared with ICG. IC7-2 was designed with similar functional groups as IC7-1, but with an unsymmetrical structure, by replacing one of the hetero-tricyclic moieties of IC7-1 with a quinoline ring, since it has previously been reported that unsymmetrical fluorogenic cyanines typically have longer wavelength emission spectra [12, 14] than the corresponding symmetrical cyanines. As expected, a longer emission wavelength (ca 900 nm) was observed for IC7-2 compared to IC7-1, which could provide superior properties for *in vivo* usage, although the quantum yield of IC7-2 was somewhat lower than IC7-1.

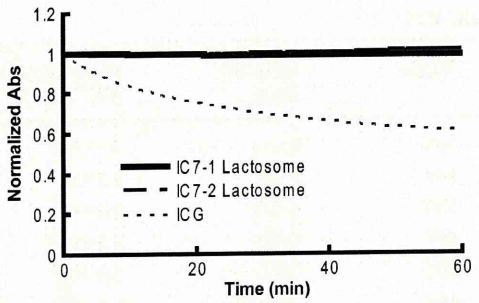

Fig. 4 Photostability of IC7-1 lactosome (*bold line*), IC7-2 lactosome (*dotted bold line*), and ICG (*dotted line*)

Multicolor *in vivo* optical imaging is a promising technique for detecting different tumor types or lymph nodes simultaneously [15, 16]. Since NIR fluorescent organic compounds that are commercially available or that have been reported for *in vivo* optical imaging have emission wavelengths in the range of 650–820 nm [17], and widely used quantum dot based agents have toxicity concerns due to associated heavy metals [18, 19], our probes with emission spectra in the 800–900 nm range offer a possible alternative for multicolor *in vivo* optical imaging.

To make IC7-1 and IC7-2 more effective for use in an aqueous environment while maintaining their optical properties, the fluorophores were encapsulated in nano-

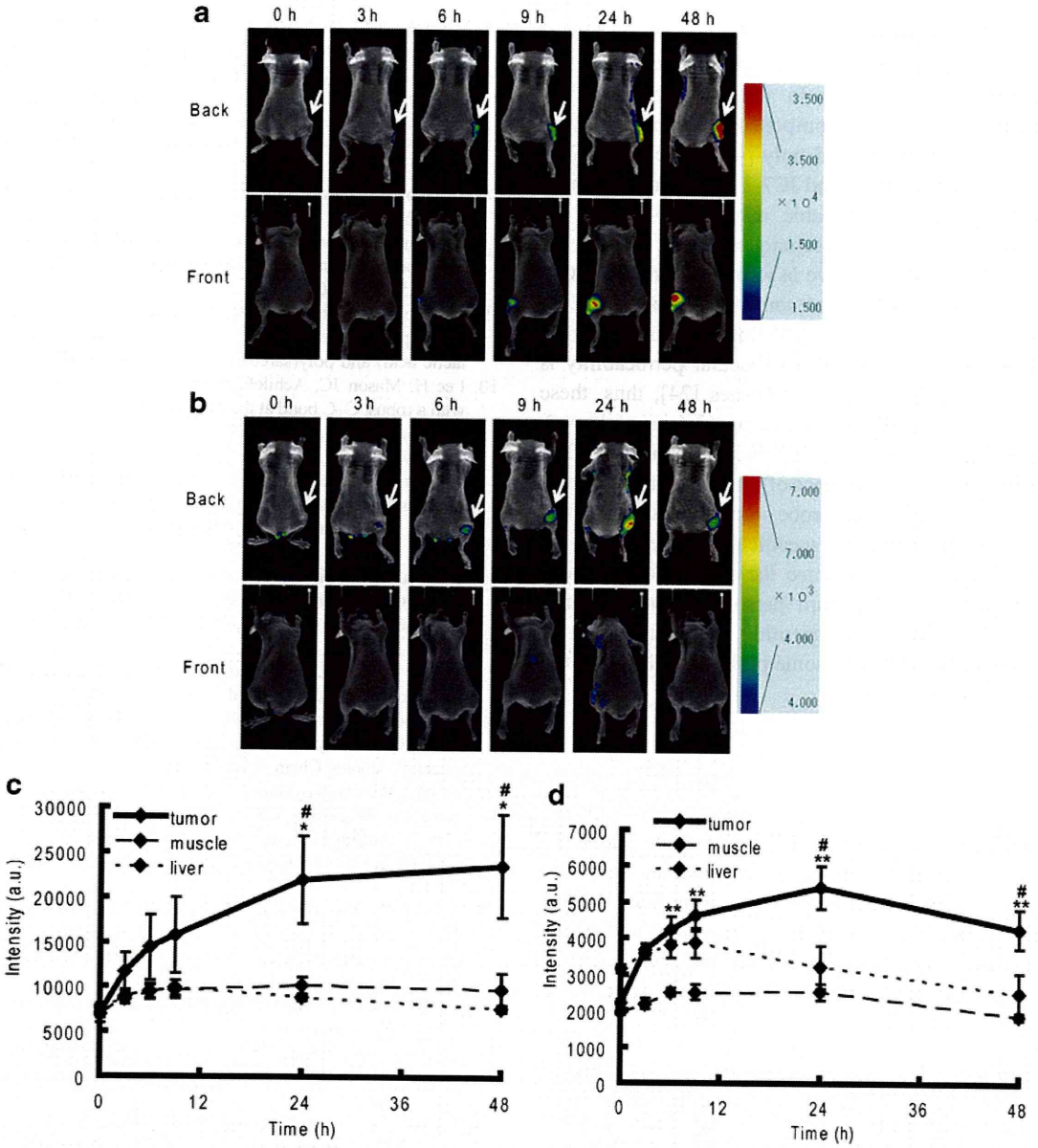

Fig. 5 **a, b** Back (*upper*) and front (*lower*) fluorescence images of FM3A cell xenografted mice at 0 h (just after injection), 3, 6, 9, 24, and 48 h after administration of IC7-1 lactosome (**a**) and IC7-2 lactosome (**b**). The *arrows* indicate the tumor (**c**, **d**). Fluorescence intensities at the region of interest of the tumor, muscle, and liver of mice administered IC7-1 lactosome (**c**) and IC7-2 lactosome (**d**). Data are expressed as fluorescence intensity (mean±S.D.). Comparisons of the fluorescence intensities of tumor and muscle or liver were performed with two-way factorial ANOVA followed by the Tukey-Kramer test (*$p<0.05$ vs. muscle, **$p<0.01$ vs muscle, $^{\#}p<0.05$ vs. liver)

carriers. As a nanocarrier for the imaging agents, we chose an amphiphilic polydepsipeptide micelle "lactosome". Lactosome has a diameter of approximately 30–40 nm, which is a suitable size for delivery to tumor tissue through the EPR effect [20]. Furthermore, lactosomes have the ability to escape the reticuloendothelial system (RES), and thus, they are able to suppress nonspecific accumulation of the probes in the abdominal region [21]. Experimental results showed that IC7-1 lactosome and IC7-2 lactosome had better quantum yields and photostability and longer (more favorable for *in vivo* imaging usage) excitation/emission wavelengths than ICG under aqueous conditions, which suggested that the high lipophilicity of IC7-1 and IC7-2 was adequate for encapsulation in lactosomes, i.e. the hydrophobic core of the lactosome provided a suitable environment for IC7-1 and IC7-2 to exert their favorable optical properties. As clearly demonstrated in the *in vivo* study, selective and pronounced signaling by the newly

developed NIR lactosome probes in tumors and low background signals in liver and muscle tissue were observed and semi-quantified. In addition, lactosome has low toxicity since it is composed of biodegradable substances, poly-sarcosine and poly-$_L$-lactic acid [22, 23]. Therefore, IC7-1 lactosome and IC7-2 lactosome appear to be promising, widely applicable nanocarrier probes for noninvasive *in vivo* imaging techniques.

In this study, highly sensitive *in vivo* tumor imaging with IC7-1 lactosome and IC7-2 lactosome by virtue of the EPR effect was achieved. Regions of inflammation are known to accumulate macromolecules since vascular permeability is facilitated compared with normal tissues [24]; thus, these probes certainly visualized such areas (data not shown). Although tumor accumulation of a probe due to the EPR effect is useful for detecting the presence of tumors and for treatment by drugs carried within the probe, functional imaging that targets functional molecules specifically expressed at the lesion site could further enhance the specific diagnosis of disease, a current trend toward personalization of patient treatment. Thus, studies concerning the conjugation of targeting moieties to the lactosome probes developed in this study are now in progress.

Conclusion

In this study, we synthesized IC7-1 lactosome and IC7-2 lactosome, which had suitable optical imaging properties and achieved clear *in vivo* tumor imaging in mice. Results from the application of IC7-1 lactosome and IC7-2 lactosome as *in vivo* imaging agents indicate that these probes could be beneficial for the clinical detection of tumors.

Acknowledgement This study was supported by Grants-in-Aid for Scientific Research from the Ministry of Education, Culture, Sports, Science, and Technology, Japan. Part of this study was supported by the New Energy and Industrial Technology Development Organization (NEDO), Japan. We thank Dojindo Laboratories (Kumamoto, Japan) for supporting the syntheses of IC7-1 and IC7-2.

References

1. Weissleder R, Pittet MJ (2008) Imaging in the era of molecular oncology. Nature 452(7187):580–589
2. Willmann JK, van Bruggen N, Dinkelborg LM, Gambhir SS (2008) Molecular imaging in drug development. Nat Rev Drug Discov 7(7):591–607
3. Ntziachristos V, Ripoll J, Wang LV, Weissleder R (2005) Looking and listening to light: the evolution of whole-body photonic imaging. Nat Biotechnol 23(3):313–320
4. Weissleder R (2001) A clearer vision for *in vivo* imaging. Nat Biotechnol 19(4):316–317
5. Dzurinko VL, Gurwood AS, Price JR (2004) Intravenous and indocyanine green angiography. Optometry 75(12):743–755
6. Landsman ML, Kwant G, Mook GA, Zijlstra WG (1976) Light-absorbing properties, stability, and spectral stabilization of indocyanine green. J Appl Physiol 40(4):575–583
7. Sakka SG (2007) Assessing liver function. Curr Opin Crit Care 13 (2):207–214
8. Makino A, Kizaka-Kondoh S, Yamahara R, Hara I, Kanzaki T, Ozeki E, Hiraoka M, Kimura S (2009) Near-infrared fluorescence tumor imaging using nanocarrier composed of poly(L-lactic acid)-block-poly(sarcosine) amphiphilic polydepsipeptide. Biomaterials 30(28):5156–5160
9. Makino A, Yamahara R, Ozeki E, Kimura S (2007) Preparation of novel polymer assemblies, "lactosome", composed of Poly(L-lactic acid) and poly(sarcosine). Chem Lett 36(10):1220–1221
10. Lee H, Mason JC, Achilefu S (2006) Heptamethine cyanine dyes with a robust C–C bond at the central position of the chromophore. J Org Chem 71(20):7862–7865
11. Strekowski L, Lipowska M, Patonay G (1992) Substitution reactions of a nucleofugal group in heptamethine cyanine dyes. Synthesis of an isothiocyanato derivative for labeling of proteins with a near-infrared chromophore. J Org Chem 57(17):4578–4580
12. Constantin TP, Silva GL, Robertson KL, Hamilton TP, Fague K, Waggoner AS, Armitage BA (2008) Synthesis of new fluorogenic cyanine dyes and incorporation into RNA fluoromodules. Org Lett 10(8):1561–1564
13. Ballou B, Ernst LA, Waggoner AS (2005) Fluorescence imaging of tumors *in vivo*. Curr Med Chem 12(7):795–805
14. Mujumdar RB, Ernst LA, Mujumdar SR, Lewis CJ, Waggoner AS (1993) Cyanine dye labeling reagents: sulfoindocyanine succinimidyl esters. Bioconjug Chem 4(2):105–111
15. Kobayashi H, Koyama Y, Barrett T, Hama Y, Regino CA, Shin IS, Jang BS, Le N, Paik CH, Choyke PL, Urano Y (2007) Multimodal nanoprobes for radionuclide and five-color near-infrared optical lymphatic imaging. ACS Nano 1(4):258–264
16. Koyama Y, Barrett T, Hama Y, Ravizzini G, Choyke PL, Kobayashi H (2007) *In vivo* molecular imaging to diagnose and subtype tumors through receptor-targeted optically labeled monoclonal antibodies. Neoplasia 9(12):1021–1029
17. Licha K (2002) Contrast agents for optical imaging. Top Curr Chem 222:1–29
18. Derfus AM, Chan CWC, Bhatia SN (2004) Probing the cytotoxicity of semiconductor quantum dots. Nano Lett 4(1):11–18
19. Kirchner C, Liedl T, Kudera S, Pellegrino T, Munoz Javier A, Gaub HE, Stolzle S, Fertig N, Parak WJ (2005) Cytotoxicity of colloidal CdSe and CdSe/ZnS nanoparticles. Nano Lett 5(2):331–338
20. Matsumura Y, Maeda H (1986) A new concept for macromolecular therapeutics in cancer chemotherapy: mechanism of tumoritropic accumulation of proteins and the antitumor agent smancs. Cancer Res 46(12 Pt 1):6387–6392
21. Senior JH (1987) Fate and behavior of liposomes *in vivo*: a review of controlling factors. Crit Rev Ther Drug Carrier Systems 3 (2):123–193
22. Gupta B, Revagadea N, Hilbornb J (2007) Poly(lactic acid) fiber: an overview. Prog Polym Sci 32(4):455–482
23. Tsai G, Lane HY, Yang P, Chong MY, Lange N (2004) Glycine transporter I inhibitor, N-methylglycine (sarcosine), added to antipsychotics for the treatment of schizophrenia. Biol Psychiatry 55(5):452–456
24. Maeda H, Wu J, Sawa T, Matsumura Y, Hori K (2000) Tumor vascular permeability and the EPR effect in macromolecular therapeutics: a review. J Control Release 65(1–2):271–284

WHHLMI rabbits with mesenteric fat accumulation are a novel animal model for metabolic syndrome.

Masashi Shiomi [a, b], Tsutomu Kobayashi [a], Nobue Kuniyoshi [a], Satoshi Yamada [a], Takashi Ito [a]

[a] Institute for Experimental Animals, and [b] Division of Comparative Pathophysiology, Kobe University Graduate School of Medicine, Kobe, Japan

Short title: Metabolic syndrome of WHHLMI rabbits

Corresponding author: Masashi Shiomi, Institute for Experimental Animals, and Division of Comparative Pathophysiology, Kobe University Graduate School of Medicine, 7-5-1, Kusunoki-cho, Chuo-ku, Kobe 650-0017, Japan

Tel: +81 78 382 6900 Fax: +81 78 382 6904 E-mail: ieakusm@med.kobe-u.ac.jp

Key words: atherosclerosis, insulin resistance, mesenteric fat accumulation, metabolic syndrome, WHHLMI rabbits

Word count in total: 5482 words

Word count in abstract: 169 words

Abstract

Objectives: To examine whether the myocardial infarction-prone Watanabe heritable hyperlipidemic (WHHLMI) rabbit with visceral fat accumulation is a new animal model for human metabolic syndrome, we examined the relation of mesenteric fat accumulation to insulin resistance, hyperlipidemia, and atherosclerosis.

Methods: Glucose tolerance tests were performed using adult-aged (11-15 months old) and middle-aged (17-21 months old) WHHLMI rabbits fed standard chow restrictedly. In addition, lipoprotein lipid levels, serum C-reactive protein levels, mesenteric fat weight, and physical and physiological parameters were measured. Mesenteric fat was stained immunohistochemically.

Results: The mesenteric adipose tissue was positive for monoclonal antibodies against macrophages, C-reactive proteins, and monocyte chemoattractant protein. In adult-aged rabbits, mesenteric fat correlated to aortic lesion area, insulin resistance, fasting immunoreactive insulin, serum C-reactive protein, abdominal circumference, and body weight. In middle-aged rabbits, mesenteric fat correlated to lipoprotein lipid levels in addition to the parameters showing a significant correlation in adult-aged rabbits but not aortic lesion area.

Conclusions: The WHHLMI rabbit with visceral fat accumulation is a new animal model for metabolic syndrome.

Introduction

Raised serum cholesterol levels are considered a major risk factor for atherosclerosis. However, hypocholesterolemic treatment is effective at preventing coronary events in less than 50% of patients [1]. Therefore, lipid abnormalities can only partly explain the prevalence of the development of coronary heart disease and the control of factors other than serum cholesterol levels is important to lower the prevalence of heart disease. Metabolic syndrome is associated with an increased risk of both diabetes and cardiovascular disease [2] and has a very high prevalence (24% in the US and between 24.6% and 30.9% in Europe) [3]. According to the International Diabetes Federation, metabolic syndrome is a disease cluster involving the accumulation of mesenteric fat (visceral fat) accompanying any two of the following: insulin resistance (or mild hyperglycemia), hypertriglyceridemia, low high-density lipoprotein (HDL) cholesterol levels, and raised blood pressure [4].

Studies using genetically modified mice and spontaneous mutant mice have contributed to the finding of adipocytokines, clarifying their role [5], and the molecular mechanism of the development of metabolic syndrome [6]. However, the lipoprotein metabolism in rodents differs markedly from that in humans [7] and there are no rodent models for metabolic syndrome with atherosclerosis, except a few mouse strains with slight atherosclerotic lesions [8,9]. Recently, a swine model for metabolic syndrome was established using an atherogenic diet [10]. This model is useful for stent experiments but the correlation between mesenteric fat accumulation and atherosclerosis is unclear. In rabbits, however, lipoprotein metabolism resembles that in humans [11,12]. The postprandial hyperlipidemic rabbit showed intraperitoneal fat accumulation, insulin resistance, and postprandial hypertriglyceridemia [13], mimicking human metabolic syndrome, although no atherosclerotic lesions developed. Recently, Waqar et al. reported that a high-fat diet induced metabolic syndrome and atherosclerosis in rabbits [14]. They clearly demonstrated that their model is similar to human metabolic syndrome. However, they did not analyze the influence of mesenteric fat accumulation or insulin resistance on plasma lipid levels or the degree of atherosclerosis.

At Kobe University, we developed the Watanabe heritable hyperlipidemic (WHHL) rabbit, an animal model of familial hypercholesterolemia [15]. WHHL rabbits show hypercholesterolemia due to a genetic defect of

low-density lipoprotein (LDL) receptors and spontaneous atherosclerosis [12]. We have also developed a myocardial infarction-prone strain (WHHLMI rabbits) by selective breeding of WHHL rabbits [16]. Some WHHL rabbits showed intraperitoneal fat accumulation and insulin resistance, and these findings were improved by a thiazolidinedione derivative, a PPAR-γ agonist [17,18], which is an insulin action enhancer. These studies suggest WHHL or WHHLMI rabbits with intraperitoneal fat accumulation to be a good animal model for examining the relation between metabolic syndrome and the development of atherosclerosis. In the present study, we examined the relation of mesenteric fat accumulation to insulin resistance, hyperlipidemia, and atherosclerosis, to examine whether the WHHLMI rabbit with mesenteric fat accumulation is a new animal model for human metabolic syndrome.

Materials and Methods

Animal care and use

We used 46 WHHLMI rabbits aged 11-15 months old (adult-age) and 52 WHHLMI rabbits aged 17-21 months old (middle-age), as well as 10 adult-aged Japanese white rabbits as a normal control. The WHHLMI rabbits were bred at the Kobe University Graduate School of Medicine. The Japanese white rabbits were obtained from Kitayama Labes, Co. Ltd. (Ina, Japan). The rabbits resided individually in metal cages (550 mm wide, 600 mm deep, and 450 mm high) with a flat metal floor, and consumed standard rabbit chow (LRC4, Oriental Yeast Co., Ltd., Tokyo, Japan) at 120 g/day and water *ad libitum*. The animal rooms were maintained under a constant temperature (22 ± 2°C), relative humidity (50–60%), ventilation rate (15 cycles/hour), and lighting cycle (12 hours light/dark). This study was approved by the Institutional Animal Care and Use Committee (approval numbers: P080111R, P091011R), and animal experiments were conducted in accordance with the Regulations for Animal Experimentation of Kobe University, the Act on Welfare and Management of Animals (Law No. 105; 1973, revised in 2006), Standards Relating to the Care and Management of Laboratory Animals and Relief of Pain (Notification No. 88, 2006), and

Fundamental Guidelines for the Proper Conduct of Animal Experiments and Related Activities in Academic Research Institutions under the Justification of the Ministry of Education, Culture, Sports, Science and Technology (Notice No.71, 2006).

Intravenous or oral glucose tolerance test

The intravenous glucose tolerance test (IVGTT) was carried out according to methods described previously [17,18]. After 16 hours' fasting, rabbits were injected with a glucose solution (0.6g/kg body weight) with a marginal ear vein. Blood samples were collected through ear veins 0, 5, 10, 20, 30, 60, and 120 minutes after the glucose was administered. The oral glucose tolerance test (OGTT) was performed as described previously [13]. After 16 hours' fasting, rabbits were administered a glucose solution (1.5 g/kg body weight) orally. Blood samples were collected through marginal ear veins 0, 15, 30, 45, 60, 90, 120, 180, and 240 minutes after the glucose administration. Blood sugar and immuno-reactive insulin (IRI) concentrations were assayed. Using fasting blood sugar and IRI levels, homeostasis model assessment insulin resistance (HOMA-IR) [19], and the Matsuda-insulin sensitivity index (ISI) [20], Matsuda and DeFrozo demonstrated that the Matsuda-ISI in OGTT well reflects whole-body insulin sensitivity [20].

Measurements of body size and blood pressure

Blood pressure in conscious rabbits was monitored directly at the ear central artery. An IV infusion catheter (18G X 2 inches, SR-FF1851, Termo, Japan) was inserted into the ear artery. A transducer (DTX Plus DT-4812, Becton Dickinson Inc., NJ, USA) was connected to the catheter via pressure tubing (TPT-12, PT-06, or PT-60, BD inc). Recordings were made with PowerLab8/SP (ADI instruments). After euthanasia by intravenous injection of pentobarbital (30 mg/kg), the abdominal circumference at the lowest part of the costal bone and length from shoulder to buttocks was measured. Mesenteric fat, axillary fat, inguinal fat, the aorta and the heart were excised.

Preparation of histological sections

After the adipose tissue and heart were weighed, they were fixed with a 10% buffered formalin solution, and embedded in paraffin. Each section was sliced serially 4 μm thick. Sections were stained immunohistochemically with monoclonal antibodies against RAM-11 (Dako A/S, Glostrup, Denmark) specific for rabbit monocytes/macrophages, MCP-1 (Dako A/S) specific for monocyte chemoattractant protein-1 (MCP-1), and CRP (Dako A/S) specific for C-reactive protein (CRP). Immunohistochemical staining was carried out using a DAKO Envision + kit according to the manufacturer's instructions, accompanied by hematoxylin counter staining.

Evaluation of atherosclerotic lesions of aorta

All parameters for atherosclerotic lesions were measured by computer-assisted color image analysis (Image-Pro Plus, version 4.5, Media Cybernetics Inc., Silver Spring, MD, USA). Aortic atherosclerosis was evaluated using the percent surface area of lesions on the whole aorta (surface area of lesion / surface area of the whole intima x 100) [21].

Preparation of plasma lipoproteins and biochemical analyses

Lipoproteins were fractionated by ultracentrifugation (very low density lipoprotein (VLDL), density <1.006 g/ml; LDL, 1.006 g/ml < density <1.063 mg/dl; HDL, density >1.063 g /ml) [22]. Total cholesterol and triglyceride levels were assayed by enzymatic methods. Blood sugar levels were assayed with Antsense III (Horiba Ltd., Kyoto, Japan). Serum insulin levels and CRP levels were assayed with ELISA kits (Rabbit CRP ELISA kit, Shibayagi Co., Ltd., Shibukawa, Japan)

Statistical analyses

Data are represented as the mean ± standard error of the mean (SEM). Statistical analyses were carried out for mean values with Student's t-test or Welch's t-test, or for the mean values among multiple groups with Scheffes' multiple comparison test, and for frequency with a chi-squared test. Correlation analyses were carried out with Pearson' correlation test. A value of $P<0.05$ was considered statistically significant.

Results

Base line data of WHHLMI rabbits

There were no significant differences in baseline data, except serum or lipoprotein lipid levels and atherosclerotic lesions, between adult-aged WHHLMI rabbits and Japanese white rabbits (Table 1). In middle-aged WHHLMI rabbits, the accumulation of fat in the mesenterium and inguinal region was increased and blood sugar levels were lowered compared with values in adult-aged WHHLMI rabbits and/or Japanese white rabbits.

Accumulation of mesenteric fat in WHHLMI rabbits

Fig. 1-A and B show the accumulation of intraperitoneal fat in middle-aged WHHLMI rabbits compared to Japanese white rabbits (Figure 1-C and D). In the mesenteric fat of WHHLMI rabbits, RAM-11-positive cells (monocytes/macrophages) were observed in swollen adipocytes with lipid (panel-E) and were positive for MCP-1 (panel -F) and CRP (panels G and H).

Glucose tolerance test

Fig. 2 shows results of glucose tolerance tests of adult-aged rabbits. Changes in blood sugar levels were similar among the three groups. After glucose administration, however, serum IRI levels were markedly high in WHHLMI rabbits with high fasting IRI levels compared to WHHLMI and Japanese white rabbits with normal fasting IRI levels. As a result, the HOMA-IR value was significantly high and the Matsuda-ISI in OGTT and IVGTT was significantly low compared to values in rabbits with normal fasting IRI levels (Panels G-H, and J-L). Similar results were observed in middle-aged rabbits (Fig. 3). These results suggest that WHHLMI rabbits with high fasting IRI levels show insulin resistance.

Correlation between mesenteric fat accumulation and other parameters

As shown in Table 2, mesenteric fat was correlated to body size and accumulation of subcutaneous fat (axillary fat + inguinal fat) in adult- and middle-aged WHHLMI rabbits. However, a significant correlation with aortic lesions was observed in only the adult-aged rabbits. Subcutaneous fat accumulation did not correlate to aortic lesion area despite showing significant correlation to parameters of body size. As shown in Table 3, mesenteric fat correlated to most blood chemical parameters, but did not correlate to blood sugar and HDL-triglyceride in middle-aged rabbits. These results may suggest that mesenteric fat accumulation affects insulin sensitivity or response, lipoprotein metabolism, and atherosclerosis. However, a significant correlation with mesenteric fat accumulation in adult-aged rabbits was observed only for fasting IRI, HOMA-IR, and serum CRP levels. Although we analyzed rabbits aged 11-15 months and 17-21 months, age did not correlate to mesenteric fat accumulation or any other parameter (data not shown) in these age ranges. Therefore, the influence of age in these analyses was minor. Similar findings were observed in correlation analyses between subcutaneous fat and metabolic parameters, except serum CRP levels.

Correlation between the index of insulin resistance in the OGTT or fasting IRI levels and other parameters

Fasting IRI levels correlated to body size, lipoprotein lipid levels and serum CRP levels in the middle-aged group but did not correlate to aortic atherosclerosis in the adult-aged group (Table 4). On the other hand, Matsuda-ISI, an index of insulin sensitivity in the OGTT, showed a significant correlation to aortic atherosclerosis in adult-aged WHHLMI rabbits ($r=-0.477$, $P=0.029$), and the ratio of whole triglyceride level / HDL-cholesterol ($r=-0.549$, $P=0.028$) and serum CRP levels ($r=-0.646$, $P<0.001$) in middle-aged WHHLMI rabbits. These results suggest that hyperinsulinemia and insulin resistance are independent in WHHLMI rabbits.

Discussion

WHHLMI rabbits with high fasting IRI levels showed an accumulation of mesenteric fat and insulin resistance even with restricted feeding on normal chow. The mesenteric fat accumulation correlated to aortic atherosclerosis, body size, insulin sensitivity, lipoprotein metabolism, and plasma CRP levels.

In WHHLMI rabbits, the accumulation of fat at the mesenterium correlated with aortic lesion area in the adult-aged group but not middle-aged group (Table 2). This difference may be due to the extremely advanced atherosclerotic lesions in the middle-aged rabbits. Actually, the percent area of lesions on the aortic surface was 75.1±3.4% in the adult-aged group and 88.2±0.8% in the middle-aged group (Table 1). In the adult-aged group, the percent area of aortic lesions was 67.3±5.7% (n=21) in rabbits with less than 60g of mesenteric fat and 84.1±3.6% (n=15) in rabbits with more than 80g of mesenteric fat (P=0.018), respectively. The age was 13.2±0.3 months in each group. These results strongly suggest that mesenteric fat accelerates the progression of aortic atherosclerosis in adult-aged rabbits. Previous studies suggested that adipocytokines derived from mesenteric fat can affect dyslipidemia, glucose metabolism, hypertension, inflammation, and thrombogenesis [23]. These secondary disorders relate to atherogenesis [5,10,23]. Although several studies demonstrated that a high-fat diet induced obesity, insulin resistance, intraperitoneal fat accumulation, and slight atherosclerosis [8-10,14], there are no studies about the correlation between mesenteric fat accumulation and atherosclerosis. In addition, Matsuzawa pointed out that mesenteric fat is an important influence on dyslipidemia and atherogenesis because it supplies free fatty acids to the liver through portal veins [24]. Since atherosclerotic lesions enlarged to cover most of the aortic surface due to hypercholesterolemia in middle-aged rabbits, the influence of mesenteric fat accumulation might be small. In adult-aged rabbits, Matsuda-ISI of OGTT correlated negatively to aortic lesions but fasting IRI levels did not. These results indicate that insulin resistance affects the progression of atherosclerosis. Although we can not explain the present results, insulin resistance may accelerate atherosclerosis through adipocytokines secreted from adipocytes of mesenteric fat [5].

In WHHLMI rabbits, mesenteric fat accumulation correlated to Matsuda-ISI, HOMA-IR, and fasting IRI levels as in other animal models reported previously [25]. Although Matsuda-ISI values of adult-aged rabbits did not correlate with mesenteric fat accumulation, those of middle-aged rabbits showed a significant correlation. The weight of mesenteric fat was 69.8±4.6 g (n=46) in adult-aged rabbits and 92.2±6.5 g (n=52) in middle-aged rabbits (P=0.006). These results suggest that insulin resistance of WHHLMI rabbits developed with an increase in mesenteric fat accumulation. In addition, our previous study demonstrated that metabolic syndrome-like

symptoms in WHHL rabbits with high fasting IRI levels were ameliorated by the administration of troglitazone, a thiazolidinedione derivative [18]. These results suggest that WHHLMI rabbits with mesenteric fat accumulation correspond to human metabolic syndrome.

In middle-aged WHHLMI rabbits, mesenteric fat correlated to apoB-containing lipoprotein lipid levels positively and HDL-cholesterol levels negatively. The mechanisms of development of dyslipidemia in patients with metabolic syndrome or obesity were summarized previously [26]. The plasma triglyceride : HDL-cholesterol ratio showed a high correlation similar to that in obese individuals showing insulin resistance [27,28]. It is well-known that HDL-cholesterol negatively correlates to cardiovascular diseases. In mice, HDL-cholesterol levels were increased by a high-fat diet [29,30] or increased or unchanged by obesity [31,32]. An increase in HDL-cholesterol levels was also observed in rat [33,34] and swine [10] models. However, HDL-cholesterol levels were decreased in normal rabbits fed a high-fat diet and overexpression of lipoprotein lipase improved insulin resistance in rabbits fed high-fat diet [35-37]. These differences in changes in HDL-cholesterol levels may be due to species differences [12]. The results of previous studies suggest that rabbit models for metabolic syndrome or insulin resistance have the advantage of both an increase in triglyceride levels and a decrease in HDL-cholesterol levels due to the progression of mesenteric fat accumulation.

In the present study, plasma CRP levels correlated to mesenteric fat accumulation in both adult-aged and middle-aged WHHLMI rabbits and to Matsuda-ISI and fasting serum IRI levels in middle-aged rabbits. In mesenteric fat, CRP and MCP-1 were positive and macrophages had infiltrated, suggesting inflammation. On the other hand, serum CRP levels did not correlate to aortic atherosclerosis. These results suggest that serum CRP levels in WHHLMI rabbits affected the progression of metabolic syndrome or insulin resistance. Similar findings were observed in patients with metabolic syndrome [38]. In rabbits fed a high-fat diet, serum CRP levels increased accompanying insulin resistance and with an increase in intraperitoneal fat accumulation [14]. In rodents, CRP was not detected in the circulation and the inflammatory marker is serum amyloid P-component instead of CRP in humans and rabbits [39]. These findings suggest the advantage of a rabbit model for metabolic syndrome.

In conclusion, since the characteristics of WHHLMI rabbits with large amounts of mesenteric fat resemble

those of human metabolic syndrome even with restricting feeding of normal chow, the accumulation of visceral fat and insulin resistance in WHHLMI rabbits may be controlled by genetic factors. WHHLMI rabbits with mesenteric fat accumulation may be a new animal model for human metabolic syndrome.

Acknowledgements

This work was supported partly by a grants-in-aid for scientific research from the Ministry of Education, Culture, Sports and Technology, Japan (20500373 and 23300157).

References

1. Delahoy PJ, Magliano DJ, Webb K, Grobler M, Liew D: The relationship between reduction in low-density lipoprotein cholesterol by statins and reduction in risk of cardiovascular outcomes: an updated meta-analysis. Clin Ther 2009;31:236-244.
2. DeFronzo RA, Abdul-Ghani M: Assessment and treatment of cardiovascular risk in prediabetes: impaired glucose tolerance and impaired fasting glucose. Am J Cardiol 2011;108:3B-24B.
3. Pais R, Silaghi H, Silaghi AC, Rusu ML, Dumitrascu DL: Metabolic syndrome and risk of subsequent colorectal cancer. World J Gastroenterol 2009;15:5141-5148.
4. Alberti KG, Zimmet P, Shaw J: IDF Epidemiology Task Force Consensus Group. The metabolic syndrome--a new worldwide definition. Lancet 2005;366:1059-1062.
5. Matsuzawa Y, Funahashi T, Kihara S, Shimomura I: Adiponectin and metabolic syndrome. Arterioscler Thromb Vasc Biol 2004; 24: 26-33.
6. Manolagas SC, Almeida M: Gone with the Wnts: beta-catenin, T-cell factor, forkhead box O, and oxidative stress in age-dependent diseases of bone, lipid, and glucose metabolism. Mol Endocrinol 2007;21:2605-2614.
7. Bergen WG, Mersmann HJ: Comparative Aspects of Lipid Metabolism: Impact on Contemporary Research and Use of Animal Models. J Nutr 2005;135:2499-2502.
8. King VL, Hatch N, Chan HW, de Beer MC, de Beer FC, Tannock LR: A murine Model of obesity with accelerated atherosclerosis. Obesity 2010: 18: 35-41.
9. Ribas V, Drew BG, Le JA, Soleymani T, Daraei P, Sitz D, Mohammad L, Henstridge DC, Febbratio MN, Hewitt SC, Korach KS, Bensinger SJ: Myeloid-specific estrogen receptor α deficiency impairs metabolic homeostasis and accelerates atherosclerotic lesion development. Proc Natl Acad Sci 2011; 108: 16457-16462.
10. Neeb ZP, Edwards JM, Alloosh M, Long X, Mokelke EA, Sturek M: Metabolic Syndrome and coronary artery disease in Ossabaw Compared with Yukatan swine. Comp Med 2010; 60: 300-315.
11. Shiomi M, Fun J: Unstable coronary plaques and cardiac events in myocardial infarction-prone Watanabe heritable hyperlipidemic rabbits: questions and quandaries. Curr Opin Lipidol 2008; 19: 631-636.

12. Shiomi M, Ito T: The Watanabe heritable hyperlipidemic (WHHL) rabbit, its characteristics and history of development: A tribute to the late Dr. Yoshio Watanabe. Atherosclerosis 2009; 207:1-7.

13. Kawai T, Ito T, Ohwada K, Mera Y, Matsushita M, Tomoike H: Hereditary postprandial hypertriglyceridemic rabbit exhibits insulin resistance and central obesity: a novel model of metabolic syndrome. Arterioscler Thromb Vasc Biol 2006;26:2752-2757.

14. Waqar AB, Koike T, Yu Y, Inoue T, Aoki T, Liu E, Fan J: high-fat diet without excess calories induces metabolic disorders and enhances atherosclerosis in rabbits. Atherosclerosis 2010; 213:148-155.

15. Watanabe Y: Serial inbreeding of rabbits with hereditary hyperlipidemia (WHHL-rabbit). Atherosclerosis 1980; 118: 81-84.

16. Shiomi M, Ito T, Yamada S, Kawashima S, Fan J: Development of an animal model for spontaneous myocardial infarction (WHHLMI Rabbit). Arterioscler Thromb Vasc Biol 2003; 23: 1239-1244.

17. Zhang B, Saku K, Hirata K, Liu R, Tateishi K, Shiomi M, Arakawa K: Quantitative characterization of insulin-glucose response in Watanabe heritable hyperlipidemic and cholesterol-fed rabbits and the effect of cilazapril. Metabolism 1994;43: 360-366.

18. Shiomi M, Ito T, Tsukada T, Tsujita Y, Horikoshi H: Combination treatment with troglitazone, an insulin action enhancer, and pravastatin, an inhibitor of HMG-CoA reductase, shows a synergistic effect on atherosclerosis of WHHL rabbits. Atherosclerosis 1999;142: 345-353.

19. Matthews DR, Hosker JP, Rudenski AS, Naylor BA, Treacher DF, Turner RC: Homeostasis model assessment: insulin resistance and beta-cell function from fasting plasma glucose and insulin concentrations in man. Diabetologia 1985;28:412-419.

20. Matsuda M, DeFronzo RA: Insulin sensitivity indices obtained from oral glucose tolerance testing. Diabetes Care 1999; 22: 1462-1470.

21. Shiomi M, Ito T, Watanabe Y, Tsujita Y, Kuroda M, Arai M, Fukami M, Fukushige J, Tamura A: Suppression of established atherosclerosis and xanthomas in mature WHHL rabbits by keeping their serum cholesterol levels extremely low: Effect of pravastatin sodium in combination with cholestyramine. Atherosclerosis 1990;

83: 69-80.

22. Shiomi M, Yamada S, Amano Y, Nishimoto T, Ito T: Lapaquistat acetate, a squalene synthesis inhibitor, changes machrophage/lipid-rich coronary plaques of hypercholesterolemic rabbits into fibrous lesions. Br J Pharmacol 2008; 154: 949-957.

23. Matsuzawa Y: Adipocytokines and metabolic syndrome. Semin Vasc Med. 2005;5:34-39.

24. Matsuzawa Y: Pathophysiology and molecular Mechanisms of visceral fat syndrome: The Japanese Experience. Diabetes Metab Rev 1997; 13: 3-13.

25. Panchal SK, Brown L: Rodent Models for Metabolic syndrome research. J Biomed Biotech 2011; 2011: 1-14.

26. Chan DC, Barrett HP, Watts GF: Dyslipidemia in visceral obesity: mechanisms, implications, and therapy. Am J Cardiovasc Drugs 2004; 4: 227-246.

27. Karelis AD, Pasternyk SM, Messier L, St-Pierre DH, Lavoie JM, Garrel D, Rabasa-Lhoret R: Relationship between insulin sensitivity and the triglyceride-HDL-C ratio in overweight and obese postmenoposal women: a MONET study. Appl Physiol Nutr Metab 2007; 32: 1089-1096.

28. Brehm A, Pfeiler G, Pacini G, Vierhapper H, Roden M: Relationship between serum lipoprotein ratios and insulin resistance in obesity. Clin Chem 2004; 50: 2316-2322.

29. Colloson KS, Maqbool ZM, Inglis AL, Makhoul NJ, Saleh SM, Bakheet RH, Al-Johi MA, Al-Rabiaj RK, Zaidi MZ, Al-Mohanna FA: Effect of dietary monosodium glutamate on HFCS-induced hepatic steatosis: expression profiles in the liver and visceral fat. Obesity 2010; 18: 1122-1134.

30. Hahn BH, Lourencço EV, McMahon M, Skaggs B, Le E, Anderson M, Iikuni N, Lai CK, LaCava A: Pro-inflammatory high-density lipoproteins and atherosclerosis are induced in lupus-prone mice by a high-fat diet and leptin. Lupus 2010; 19:913-917.

31. Suzuki M, Kakuta H, Takahashi A, Shimano H, Tada-Iida K, Yokoo T, Kihara R, Yamada N: Effects of atorvastatin on glucose metabolism and insulin resistance in KK/Ay mice. J Atheroscler Thromb 2005; 12: 77-84.

32. Silver DL, Jiang XC, Tall AR: Increased high density lipoprotein (HDL), defective hepatic catabolism of

Apo-A1 and Apo-AII, and decreased Apo-AI mRNA in ob/ob mice. Possible role of leptin in stimulation of HDL turnover. J Biol Chem 1999; 274: 4140-4146.

33. Hikita M, Bujo H, Yamazaki K, Taira K, Takahashi K, Kobayashi J, Saito Y: Differential expression of lipoprotein lipase in tissues of the rat model with visceral obesity and postprandial hyperlipidemia. Biochem Biophys Res Commun 2000; 277: 423-429.
34. Elam MB, von Wronski MA, Cagen L, Thorngate F, Kumar P, Heimberg HG: Lipoprotein alterations in 10- and 20-week-old Zucker diabetic fatty rats: hyperinsulinemic versus insulinopenic hyperglycemia. Metabolism 1998; 47: 1315-1324
35. Kitajima S, Morimoto M, Liu E, Koike T, Higaki Y, Taura Y, Mamba K, Itamoto K, Watanabe T, Tsutsumi K, Yamada N, Fan J: Overexpression of lipoprotein lipase improves insulin resistance induced by a high-fat diet in transgenic rabbits. Diabetologia 2004; 47: 1202-1209.
36. Koike T, Liang J, Wang X, Ichikawa T, Shiomi M, Liu G, Sun H, Kitajima S, Morimoto M, Watanabe T, Yamada N, Fan J: Overexpression of lipoprotein lipase in transgenic Watanabe heritable hyperlipidemic rabbits improves hyperlipidemia and obesity. J Biol Chem 2004; 279: 7521-7529.
37. Liu E, Kitajima S, Higaki Y, Morimoto M, Sun H, Watanabe T, Yamada N, Fan J: High lipoprotein activity increases insulin sensitivity in transgenic rabbits. Metabo Clin Exper 2005; 54: 132-138.
38. Devarj S, Singh U, Jialal I: Human C-reactive protein and the metabolic syndrome. Curr Opin Lipidol 2009; 20: 182-189.
39. Pepys MB, Baltz M, Gomer K, Davies AJ, Doenhoff M: Serum amyloid P-component is an acute-phase reaction in the mouse. Nature 1979; 278: 259-261.